Biogeosciences Discuss., 8, 4871–4916, 2011
www.biogeosciences-discuss.net/8/4871/2011/
doi:10.5194/bgd-8-4871-2011

Biogeosciences Discussions

Influence of intense scavenging on Pa-Th fractionation in the wake of Kerguelen Island (Southern Ocean)

C. Venchiarutti[1,2,*], M. Roy-Barman[3], R. Freydier[4,*], P. van Beek[2], M. Souhaut[2], and C. Jeandel[2]

[1]Alfred Wegener Institute, Am Handelshafen 12, 27570 Bremerhaven, Germany
[2]LEGOS, CNRS/UMR5566, Observatoire Midi-Pyrénées, 14 Avenue Edouard Belin, 31400, Toulouse, France
[3]LSCE/IPSL Laboratoire CNRS/CEA/UVSQ, Domaine du CNRS, Bât 12, Avenue de la Terrasse, 91198 Gif-sur-Yvette Cedex, France
[4]LMTG, Observatoire Midi-Pyrénées, 14, venue Edouard Belin, 31400 Toulouse, France
[*]now at: Laboratoire HydroSciences Montpellier, Université Montpellier 2, Place Eugène Bataillon, 34095 Montpellier, Cedex 5, France

Received: 14 April 2011 – Accepted: 21 April 2011 – Published: 17 May 2011

Correspondence to: C. Venchiarutti (cvenchiarutti@gmail.com)

Published by Copernicus Publications on behalf of the European Geosciences Union.

Abstract

Dissolved and particulate excess ^{230}Th and ^{231}Pa concentrations (noted $^{230}Th_{xs}$ and $^{231}Pa_{xs}$, respectively) and $^{231}Pa_{xs}/^{230}Th_{xs}$ activity ratios were investigated on and out of the Kerguelen plateau (Southern Ocean) in the framework of the KErguelen Ocean and Plateau compared Study project in order to better understand the influence of particle flux and particle chemistry and advection on the scavenging of ^{231}Pa.

In the wake of Kerguelen Island, the relative abundance of $^{231}Pa_{xs}$ in the particles compared to the dissolved phase associated with a low fractionation factor between ^{230}Th and ^{231}Pa ($F_{Th/Pa}$ ranging from 0.06 ± 0.01 to 2.13 ± 0.63) is consistent with particles being dominated by biogenic silica in this area. Strong ^{231}Pa concentration gradients occur on relatively short distances.

Along the eastern escarpment of the Kerguelen plateau, an intensive scavenging affects significantly the dissolved distribution of $^{231}Pa_{xs}$ at depth, as already observed for $^{230}Th_{xs}$. This local boundary scavenging was attributed to re-suspension of opal-rich particles by nepheloid layers, resulting in fractionation factors $F_{Th/Pa} \leq 1$ along the Kerguelen plateau slope. Therefore, these results showed that in the Kerguelen wake, both the composition (biogenic opal) and the flux (intensive along the margin) of particles control the scavenging of the two radionuclides.

The modelling of ^{231}Pa distribution with an advection-scavenging model demonstrate that lateral advection of open ocean water on the Kerguelen plateau could supply most of the ^{231}Pa, which is then efficiently scavenged on the highly productive plateau, as previously proposed for $^{230}Th_{xs}$. It stresses that lateral advection can play a significant role in the overall budget of particle reactive trace elements in a coastal-open ocean system.

BGD
8, 4871–4916, 2011

1 Introduction

The Kerguelen plateau (South Indian Ocean) is an ideal laboratory to study the mechanisms of natural iron fertilization in the Ocean. Better defining these mechanisms was the main aim of the KErguelen Ocean and Plateau compared Study project (KEOPS, Blain et al., 2007). For this purpose, a good understanding of the particle dynamics and advection processes in this area was required.

^{231}Pa and ^{230}Th are natural radionuclides, uniformly produced in seawater by the decay of the homogeneously distributed uranium isotopes (^{235}U and ^{234}U, respectively). Consequently, they are both produced at a fixed known rate in the ocean with a production activity ratio ^{231}Pa/^{230}Th of 0.093. Both radionuclides are particle reactive and therefore rapidly adsorbed onto settling particles and removed (scavenged) from the water column to the sediment. However, their affinity for particles differs, ^{230}Th adsorption coefficients being generally 10 times higher than ^{231}Pa coefficients (Anderson et al., 1983a; Moran et al., 2002; Chase et al., 2003). Consequently, ^{231}Pa has a residence time in the water column of 50–200 yr, longer than the 10–40 yr residence time of ^{230}Th (Anderson et al., 1983a; Nozaki et al., 1985; Walter et al., 1997), so that these two radionuclides are fractionated in seawater compared to the production ratio. ^{231}Pa is transported to areas of high particle fluxes (e.g. margins) prior to being scavenged. In contrast, ^{230}Th is mainly scavenged on its production site (Walter et al., 1997; Yu et al., 2001). This enhanced scavenging at ocean margins is named "boundary scavenging" (Spencer et al., 1981; Anderson et al., 1990). Boundary scavenging is the result of the combination of i) an increasing particle flux (particle flux effect) from the open ocean to the margin and possibly from a change in particulate matter composition (particle composition effect) and ii) a sufficiently long scavenging residence time of the element (e.g. ^{210}Pb, ^{231}Pa, ...) in the open ocean so that it can be transported from the open ocean where it is produced, to the ocean margins where it is efficiently scavenged.

The ^{231}Pa distribution in the water column is governed by reversible scavenging. In other words, continuous exchanges are occurring between dissolved and solid phases

BGD
8, 4871–4916, 2011

along depth (Bacon and Anderson, 1982). The same processes control ^{230}Th distribution. Therefore, in absence of lateral transport of these radionuclides by currents, reversible scavenging yields linear increases with depth of total (dissolved + particulate) ^{231}Pa and ^{230}Th concentrations at least down to 1000 m depth (Nozaki et al., 1985; Roy-Barman et al., 1996; Choi et al., 2001; Marchal et al., 2007). Deeper in the water column, deviations from this linearity are often observed. This depletion can be due to either i) depleted surface waters that are sinking and mixing with deep waters, leading to modifications of the linear distribution for a concave shape (Rutgers van der Loeff and Berger, 1993; Vogler et al., 1998; Coppola et al., 2006) or ii) intensification of the local scavenging, leading to the depletion of the radionuclide concentrations in the deepest part of the water column (Moran et al., 2002; Venchiarutti et al., 2008; Roy-Barman 2009).

Both radionuclides are therefore mainly used as tracers for particle scavenging (Nozaki et al., 1981; Bacon and Anderson, 1982; Luo et al., 1995) but also for the deep ocean circulation or ventilation (Rutgers van der Loeff and Berger, 1993; Scholten et al., 1995; Moran et al., 1997). However, data on the distributions of ^{231}Pa and ^{230}Th in seawater and particles are still scarce, precluding a full understanding on these radionuclides oceanic behaviour.

For instance, the role of particle composition on the radionuclides scavenging remains unclear. Indeed, ^{231}Pa appears to be more reactive with inorganic particles (Fe_2O_3, MnO_2) or biogenic silica (opal) in carbonate-depleted areas, like in the Southern Ocean (Guo et al., 2002; Chase et al., 2002 and 2004; Scholten et al., 2005). Consequently, in presence of particles rich in Fe_2O_3, MnO_2 or biogenic silica, both ^{230}Th and ^{231}Pa would be adsorbed onto the particles with almost the same efficiency, thereby yielding almost no fractionation between ^{231}Pa and ^{230}Th (Walter et al., 1999; Chase et al., 2002). However, questions still remain concerning the exact affinity of these radionuclides according to particle type, grain size and whether they are adsorbed or rather incorporated in the particles.

BGD
8, 4871–4916, 2011

Moreover, recent debates question the relevance of $^{231}Pa/^{230}Th$ ratio as a circulation tracer. Indeed, it appears that the $^{231}Pa/^{230}Th$ could reflect the influence of the surrounding biological productivity (in particular diatoms) rather than the circulation imprint (Bradtmiller et al., 2006, 2009; Hayes et al., 2011), and questions still remain concerning the effect of ocean margins on the $^{231}Pa/^{230}Th$.

Here, we present the ^{231}Pa distributions in both solid and dissolved phases as well as the $^{231}Pa/^{230}Th$ fractionation in the Kerguelen area during the KEOPS program. A salient feature of this area is the biogeochemical contrast between the Kerguelen plateau and the open-ocean (phytoplankton bloom versus High Nutrient Low Chlorophyll -HNLC- area). This study complements the work on ^{230}Th during KEOPS (Venchiarutti et al., 2008) which pointed out that:

- Using the "classical" 1-D scavenging model does not allow obtaining realistic ^{230}Th scavenging rates over the Kerguelen plateau. Realistic scavenging rates were obtained by using a new advection-scavenging model that takes into account both ^{230}Th scavenging and advection of HNLC open-ocean waters over the productive plateau.

- Using this model, Venchiarutti et al. (2008) demonstrated that scavenging is strongly enhanced on the plateau and along its eastern flank (mean settling speed of small particles one order of magnitude larger than in the open ocean) and that, despite this strong increase of scavenging compared to the open ocean, the ^{230}Th concentration does not drop down to zero because the continuous inflow of open ocean water brings new ^{230}Th on to the plateau.

- Enhanced scavenging of ^{230}Th on the plateau and along its eastern flank was tentatively attributed to the occurrence of particle re-suspension by nepheloid layers.

Venchiarutti et al. (2008) also showed that the Kerguelen plateau represents an ideal "simple" case to study boundary scavenging because there is a high gradient of particle flux over a limited distance linked to a well constrained circulation over the

BGD
8, 4871–4916, 2011

plateau. As mentioned earlier, ^{231}Pa is more prone to boundary scavenging than ^{230}Th. Consequently, a significant boundary scavenging of ^{231}Pa is expected over the Kerguelen plateau.

Analysing ^{231}Pa in this area should also bring constraints on Pa/Th fractionation during scavenging processes. In particular, precise budgeting of the advection and scavenging flux using the Kerguelen boundary scavenging model should allow elucidation of the respective influence of the particle flux versus chemistry effects, a question still in debate.

Thus, the first aim of the present study is to determine if the intense scavenging highlighted by ^{230}Th on the Kerguelen plateau and along the eastern slope (Venchiarutti et al., 2008) also affects ^{231}Pa distribution. If the model proposed for ^{230}Th does not account correctly for ^{231}Pa, it would indicate processes allowing the decoupling of the two elements. The other aim is to study the fractionation of these two radionuclides in this contrasted environment, based on ^{231}Pa partition coefficients (K_d) and the ^{231}Pa/^{230}Th fractionation factor ($F_{Th/Pa}$). The results are then compared with biogenic silica (BSi) and Rare Earth Elements (REEs) that were also analysed in the context of KEOPS (Mosseri et al., 2008; Zhang et al., 2008a) in order to determine the role of particle composition on the sedimentary Pa/Th ratios.

2 Sampling and analytical methods

2.1 Regional settings: hydrography

The Southern Ocean is the largest HNLC area in the world Ocean (Sarmiento et al., 1998; Tréguer and Pondaven, 2002; Marinov et al., 2006). However, most of the islands of this ocean experience intense summer phytoplankton blooms (Pollard et al., 2009; Frew et al., 2006). In the case of the Kerguelen Island and plateau zone, a large bloom extends yearly South of the Polar Front (PF, Fig. 1) over the Kerguelen plateau, to which it is restrained by the bathymetry and surrounding HNLC waters (Blain et al., 2007; Mongin et al., 2008).

BGD
8, 4871–4916, 2011

The Kerguelen plateau divides the Antarctic Circumpolar Current (ACC) into a northern flow, north of the Kerguelen Island and a southern flow, through the Fawn Trough, delimiting the so called "central Kerguelen plateau" (Park et al., 2008a; Mongin et al., 2008). This latter extends therefore from the Kerguelen Island (north of the PF) to the Heard/McDonald Islands, its southern limit (Fig. 1). It is shallower than ∼ 560 m, with some shallow seamounts and is delimited by deeper troughs and ridges (Park et al., 2008a; Mongin et al., 2008): at north, the PF Trough (∼ 650 m) and south, the Fawn Trough (∼ 2650 m) and along the south-eastern part of the plateau, the Northwest–Southeast Trough (∼ 600 m).

LADCP measurements (Park et al., 2008a) highlighted the contrast between the weak geostrophic circulation of the shallow plateau, with a general northward flow $\leq 5\,\mathrm{cm\,s^{-1}}$ and the circulation along the eastern flank of the plateau, where a strong north-westward branch ($\sim 18\,\mathrm{cm\,s^{-1}}$) of the Fawn Trough Current brings Antarctic waters, likely originating from the eastern Enderby Basin (Fig. 1).

During the KEOPS cruise in the Austral summer 2005, three transects were covered on and out of the central Kerguelen plateau, stations numbered from 1 to 8 and 9 to 11, respectively (Fig. 1). Station A3 was then located in the core of the large bloom on the central plateau, whereas the off-plateau stations Kerfix, A11, B11 and C11 were considered as open-ocean stations in HNLC waters (Fig. 1). The bloom was mostly dominated by large diatoms in surface waters, and sediments on the plateau were dominated by siliceous ooze (Armand et al., 2008). The export of particulate carbon on the Kerguelen plateau was found to be almost double that in the surrounding HNLC waters (Savoye et al., 2008). Bacterial activity in the upper 125 m depth of the plateau was higher than in the HNLC area whereas the inverse was observed for the mesopelagic layer (Obernosterer et al., 2008; Jacquet et al., 2008). This difference was attributed to the occurrence of larger diatoms cell sizes on the plateau than in the HNLC waters.

BGD
8, 4871–4916, 2011

Finally, Zhang et al. (2008b), van Beek et al. (2008) and Chever et al. (2010) demonstrated that waters originating from further south of the Kerguelen plateau and spreading northward over the plateau, were likely enriched in trace elements due to shelf weathering in the vicinity of Heard Island. These advected waters may be an important source of trace elements to the Kerguelen plateau and contribute significantly to the natural fertilisation.

2.2 Sampling

The full sampling and preparation procedures – common for both radionuclides – are fully detailed in Venchiarutti et al. (2008). Below we will summarize only briefly some specific treatments related to the Pa analysis.

Seawater samples were collected during KEOPS cruise on board the R/V Marion Dufresne (19 January 2005–13 February 2005, Fig. 1) using General Oceanics 12 L-Niskin bottles and a Seabird SBE19+CTD at 6 stations: on (A3 and C1) and off (Kerfix, A11, B11 and C11) the Kerguelen plateau. The core of the bloom (station A3) was sampled twice within 2 weeks interval for the radionuclide analysis (referred as A3–33 for the first visit and A3-77 for the second).

Briefly, the 30 l-seawater samples were first filtered through 47 mm diameter Millipore filters (0.65 µm Durapore or 0.8 µm Versapore), spiked with the corresponding yield tracers, 50 pg of ^{229}Th and ca. 140 fg of ^{233}Pa (produced by neutron activation of ^{232}Th). After 12 h equilibration, both radionuclides were co-precipitated, with $KMnO_4$ and $MnCl_2$ solutions, by addition of NH_4OH, based on the protocol of Rutgers van der Loeff and Moore (1999). After 24 h homogenisation, the samples were filtered through 142 mm diameter Millipore membranes and the filters stored in Petri-dishes.

Particle samples were collected using in situ pumps (McLane and Challenger Oceanic systems) at 6 out of 9 stations. At each station, 83-2564 L were filtered in situ through 0.65 µm Durapore or 0.8 µm Versapore filters (diameters of 142 or 293 mm) and the filters were folded and stored in Petri-dishes to be analysed once back at the home laboratory.

BGD
8, 4871–4916, 2011

2.3 Analytical procedures

All the analytical procedures were conducted using acid-cleaned containers and materials, double-distilled reagents, and the analyses were performed in clean-rooms (Class Iso 5–6) at the home laboratory LEGOS.

2.3.1 Dissolved samples

The Mn-filter precipitates were leached in 9 M HCL baths. After evaporation of the leaching solution to almost dryness, the samples were spiked with ^{236}U (~ 40 pg) to trace ^{233}U bleeding in the Pa fraction (Choi et al., 2001). Th and Pa were separated and purified using an anion exchange resin (AG1x8, 100–200 mesh). The elution steps are further documented in Venchiarutti et al. (2008) and Jeandel et al. (2011). We assumed that we obtained good chromatographic recoveries for the whole Pa samples, based on the typical Pa recoveries obtained with this column (97.9 ± 0.7 %, $n = 2$, see also Jeandel et al., 2011).

Due to technical reasons, the co-precipitation recovery could not be determined except for the samples collected at A3-33, for which we estimated an average co-precipitation recovery from the analysis of the filters using gamma-spectrometry measurements achieved at the LSM (Laboratoire Souterrain de Modane, French Alps). The filters were counted for gamma spectrometry before being leached. The co-precipitation recovery was 103 ± 11 % for nine A3-33 samples (Table 1). This good recovery was encouraging and we assumed then that the co-precipitation step has been as efficient at all the sampled KEOPS stations as at A3-33.

The ^{231}Pa analysis of the stations Kerfix, A11 and A3-33 was achieved within six months after the expedition. However, the rapid decay of the ^{233}Pa spike ($T_{1/2}$ = 26.967 ± 0.004 days, Regelous et al., 2004) prevented us from using the isotope dilution technique for these samples. Therefore, ^{231}Pa concentrations were obtained by external calibration on a Finnigan Neptune MC-ICPMS, i.e. by comparing the 231 beam from a ^{231}Pa standard with the ^{231}Pa beam/signal measured in each sample, thereby

BGD
8, 4871–4916, 2011

preventing us to estimate an accurate overall chemistry recovery at these three stations.

Afterwards, because of a 4-month mass spectrometer breakdown, the analysis of 4 other remaining stations (stations A3-77, B11, C11 and C1) was postponed for almost one year and consequently, no ^{233}Pa spike remained at all in these samples. Finally, the Mn-filter precipitates at these four stations were split into two aliquotes (each equivalent to 15 L seawater), to enable initially the Th analysis in one aliquote (Venchiarutti et al., 2008) and later, after re-spiking with a new ^{233}Pa spike (prepared by milking a solution of ^{237}Np) in the other aliquote, the ^{231}Pa concentrations of these samples could be determined by isotope dilution (i.e. using the ^{233}Pa/^{231}Pa ratio measured in each sample).

These analytical drawbacks were taken into account in the error bar estimates (see Sect. 2.4.3) and yielded a cautious interpretation of our data.

2.3.2 Particle samples

The ^{231}Pa and Th particulate samples were leached in a mixture of concentrated HCl and HNO_3 followed by the addition of Suprapur HF, based on the protocols given in Tachikawa et al. (1997) and Venchiarutti et al. (2008). The particle analysis was performed on 20 % aliquots for Th isotopes and 80 % for ^{231}Pa. After spiking with the corresponding yield tracers, 15 pg of ^{236}U were added in the 80 % aliquots dedicated to the ^{231}Pa analysis.

Th and Pa were then separated and purified through the same anion exchange resin described in Venchiarutti et al. (2008).

2.4 Spectrometric analysis

After the chromatographic separation, ^{230}Th and ^{231}Pa purified fractions were measured within 24 h (so that ^{233}Pa decay to ^{233}U is minimal, see Sect. 2.4.2) in a 2 % HNO_3 solution on a Finnigan Neptune MC-ICPMS (Observatoire Midi-Pyrénées,

BGD
8, 4871–4916, 2011

Toulouse) and their concentrations calculated by isotope dilution from the measured $^{229}Th/^{230}Th$ and $^{233}Pa/^{231}Pa$ ratios.

Th isotope measurement is further detailed in Roy-Barman et al. (2005) and Venchiarutti et al. (2008). Pa analysis was performed according to the protocols derived from Choi et al. (2001) and Regelous et al. (2004). Pa samples were introduced into the plasma through a Cetac Aridus system, equipped with a PFA microflow nebulizer (Elemental Scientific, 50 µL min^{-1}) and a membrane desolvator, resulting in a passive sample uptake (without peristaltic pump) of ~ 60 µL min^{-1}. This system was optimized using N_2 (flow rate of 5 ml min^{-1}) and Ar (sweep gas, flow rate of ~ 10 ml min^{-1}) gases.

Before each sequence for Pa measurements, the instrument was tuned and peak shapes were improved, for both Faraday cups and SEM, using a standard solution of natural U (SRM 4321 C), with a certified $^{238}U/^{235}U$ ratio of 139.67 ± 0.016. This U solution was also run every eight samples in order to bracket the samples and check the instrument short and long-term variability and mass bias (linear correction) during the analysis.

To prevent from any cross-contamination (carry-over) between samples, the system was thoroughly cleaned with a 2 % HNO_3 v/v solution after each sample run and acid blanks were run prior to each measurement.

2.4.1 Corrections for ^{232}Th tailing and isobaric interferences

The importance of ^{232}Th tailing correction for masses 230 and 231 have been previously underlined by Choi et al. (2001), Pichat et al. (2004) and Thomas et al. (2006). However, tailing effect might be attenuated for seawater samples because the ^{232}Th concentration is generally low. Nevertheless, the abundance sensitivity or tailing correction has to be checked for each sample and particularly for ^{231}Pa measurement owing to its low concentrations. We therefore applied a linear correction based on the systematic measurements of the masses 229.5 and 230.5 for ^{230}Th, 230.5 and 231.5 for ^{231}Pa, as previously done by Choi et al. (2001). The abundance sensitivity of the MC-ICP-MS at the time of the Pa analyses was ~ 0.3 ppm for masses 2 amu apart (i.e.

BGD
8, 4871–4916, 2011

on ^{230}Th peak, with the Retarding Potential Quadrupole lens- RPQ settings at this time) and ~2 ppm for masses 1 amu apart, i.e. for the ^{231}Pa peak. However, thanks to an efficient chromatographic separation, leaving typically less than 2.5 ± 1.6 % of ^{232}Th in the Pa fraction (Jeandel et al., 2011), the ^{231}Pa/^{232}Th ratio in the samples was typically of ~ 1×10^{-3} (except in one sample for which ^{231}Pa/^{232}Th = 7×10^{-4}).

Isobaric interferences from hydride formation (^{232}Th^{1}H), that can affect ^{233}Pa measurements, were significantly limited when using the membrane desolvatation and low sample uptake of ~ 60 µl min^{-1} (Choi et al., 2001; Pichat, 2001; Regelous et al., 2004). We measured the 233/232 ratios for different ^{232}Th concentrations (0.25–5 ng g^{-1}): values varied from 0.48×10^{-5} to 1×10^{-5} comparable to the 233/232 ratio of 0.95×10^{-5} found by Choi et al. (2001) on a HR-ICP-MS for a similar range of ^{232}Th concentrations.

For KEOPS samples, most of the ^{232}Th concentrations in seawater (Venchiarutti et al., 2008) were typically lower than 100 pg kg^{-1} (except for a few samples, notably at C1), so that the highest measurable ^{232}Th and ^{233}Pa quantities (for a 15 L sample) were typically lower than 1.6 ng (0.8 ng g^{-1} in 2 ml) and 140 fg, respectively. Moreover, the efficient column separation of Th and Pa allows us to limit the percentage of ^{232}Th "bleeding" (< 2.5 %) in the Pa fraction, thereby inducing a ^{233}Pa/^{232}Th ratio < 3.73×10^{-3} in the samples. Consequently, taking the highest ^{232}Th^{1}H/^{232}Th ratio = 1×10^{-5} yields to a hydride correction typically < 0.3 %. Note that some of the highest ^{232}Th concentrations (Venchiarutti et al., 2008) were found at stations A3-33, Kerfix and A11, for which no ^{233}Pa measurement was used in the calculation of ^{231}Pa concentrations, as described in Sect. 2.3.1 and therefore for which, such hydride correction was not necessary.

2.4.2 Corrections for uranium bleeding and in-growth

Adding ^{236}U to the seawater and particulate samples prior to the anion exchange column allowed us to monitor the efficiency of the column separation of U and Pa, and thus to ensure that the Pa fraction is free of any ^{233}U. Indeed, the presence of any ^{233}U

BGD
8, 4871–4916, 2011

in the Pa fraction or so called "^{233}U bleeding" would interfere the counting on mass 233 (Choi et al., 2001; Pichat et al., 2004).

Our chromatographic separation is efficient with insignificant residual U amount in the Pa fraction (less than 0.01 % of the total U). Nevertheless the contribution of ^{233}U bleeding on the 233 peak in the Pa fraction was checked and estimated following Eq. (1):

$$n^{233}\mathrm{Pa}_{\mathrm{final}} = n^{233}(\mathrm{Pa,U})_{\mathrm{sple}} - \left\{ \left(\frac{n^{236}\mathrm{U}_{\mathrm{sple}}}{n^{236}\mathrm{U}_{\mathrm{spike}}} \right) \times n^{233}(\mathrm{Pa,U})_{\mathrm{sple}} \right\} \quad (1)$$

Where n is the number of counts on the masses 233 and 236, and the sub-scripts sple and spike referred to sample (the Pa fraction) and ^{236}U spike, respectively. The estimate of bleeding is based here on the counts of uranium found in the Pa fraction and not on the measurements of the U ratios in the U fractions, preventing us to compare to the literature values (Choi et al., 2001; Pichat et al., 2004; Thomas et al., 2006). Most of our Pa analyses were not affected by the bleeding, except 10 samples, for which a ^{233}U bleeding ranged from 0.5 % to 11 % and the aforementioned correction (Eq. 1) was applied.

All the dissolved ^{230}Th and ^{231}Pa samples were corrected for the in-growth from the uranium, which was co-precipitated with MnO_2, assuming a maximum of 5 % of co-precipitated U in the samples (Roy-Barman, personal communication). The mean U-decay corrections represent up to 0.04 % (mostly in surface water at A3-33, measured 137 days after sampling) and 1.1 % (A3-77, measured 827 days after sampling) in the Pa and Th samples, respectively.

2.4.3 Uncertainties and blanks

For the Pa samples at stations Kerfix, A11 and A3-33, the final uncertainty was estimated taking into account the errors on acid blanks, ^{232}Th tailing, co-precipitation recovery, chemical blanks and finally assuming a 10 % error on the ^{231}Pa standard

BGD
8, 4871–4916, 2011

concentration and on the ^{233}Pa spike (i.e. that encompasses errors on initial activity and ^{231}Pa contribution from the spike). At the other four stations (A3-77, B11, C11 and C1), uncertainties for ^{231}Pa concentrations were propagated at the 2σ level and include the instrument statistical error, carry-over correction, mass bias, spike contributions and overall procedural blanks. Corrections, described in the previous sections, for the ^{232}Th tailing and ^{233}U bleeding were also taken into account.

For the dissolved samples, the procedural blanks (Table 2) were estimated by analysing (as for a sample) the co-precipitated filters (of two types: Durapore and Versapore) achieved on-board, using 10 L ultra-pure water and the same reactants and reagents as for the samples. Distinguishing contamination due to the use of one type of filters with respect to the other was not statistically significant. The blanks for the particles (Table 2) were achieved using Versapore filters. They were generally close to the background noise. The detection limit was estimated at 1.2 fg of ^{231}Pa and corresponds to three times the standard deviation based on two blanks for particles ($N = 2$).

Although we could not establish a significant statistic on our blank values, they are in the range of those gathered from the literature (Choi et al., 2001; Moran et al., 2002; Edmonds et al., 2004) whatever the extraction method (co-precipitation with Fe or Mn-Ox, filtration or siphoning-off).

The overall yields obtained for Th isotopes and ^{231}Pa are reported in Table 1 and are in the range previously reported in the literature (Choi et al., 2001; Thomas et al., 2006).

3 Results

In seawater, most of the ^{230}Th and ^{231}Pa are produced by the radioactive decay of the soluble and homogeneously distributed ^{234}U and ^{235}U, respectively, providing the authigenic fraction of these radionuclides in any given sample. However, an accurate determination of this fraction requires the correction of the measured value from the detrital contribution which is supported by the U already contained in the particles.

BGD
8, 4871–4916, 2011

This latter is the lithogenic fraction of these radionuclides in the same sample. The lithogenic contribution can be critical in areas receiving strong lithogenic inputs.

Here, we estimated the ^{230}Th and ^{231}Pa scavenged from seawater and termed as "unsupported" (or in excess) $^{230}Th_{xs}$ and $^{231}Pa_{xs}$, following the Eqs. (2) and (3):

$$^{230}Th_{xs} = {}^{230}Th_{measured} - {}^{232}Th_{measured} \times \left(\frac{^{230}Th}{^{232}Th}\right)_{litho} \quad (2)$$

Where $(^{230}Th/^{232}Th)_{litho} = 4.4 \times 10^{-6}$ mol mol^{-1} based on Roy-Barman et al. (2002).

$$^{231}Pa_{xs} = {}^{231}Pa_{measured} - \left(\frac{^{235}U}{^{238}U}\right)_{natural} \times \left(\frac{^{238}U}{^{232}Th}\right)_{litho} \times {}^{232}Th_{measured} \quad (3)$$

The mean natural activity ratio $^{235}U/^{238}U$= 0.04605 (Scholten et al., 1995, 2005; Moran et al., 2005) is applied in Eq. (3), $^{238}U/^{232}Th$ crustal activity ratio has been measured in different locations and varies from 0.8 ± 0.2 (Anderson et al., 1990) in the Pacific, 0.7 ± 0.2 in the Atlantic (Scholten et al., 2008) and 0.4 ± 0.1 south of the Antarctic Polar Front (Walter et al., 1997). We used here a value of $^{238}U/^{232}Th = 0.8 \pm 0.2$ (Anderson et al., 1990) to estimate $^{231}Pa_{xs}$ in the wake of Kerguelen.

Dissolved and particulate $^{231}Pa_{xs}$ concentrations on and off the Kerguelen plateau are reported in Tables 3 and 4 respectively and in Figs. 2, 5 and 9 and expressed in dpm m^{-3}. All the $^{231}Pa_{xs}/^{230}Th_{xs}$ ratios reported in Tables 3 and 4 and represented in Figs. 3–4 are activity ratios.

Most of the dissolved $^{231}Pa_{xs}$ concentrations and $^{231}Pa_{xs}/^{230}Th_{xs}$ ratios are in the range previously observed in the South-West Indian Basin (Thomas et al., 2006), in the Equatorial Atlantic (Choi et al., 2001; Moran et al., 2002) or in the South Atlantic (Rutgers van der Loeff and Berger, 1993; Walter et al., 2001).

Radionuclide concentrations in particles (Tables 3 and 4) are consistent with values found in the Labrador Sea (Moran et al., 2002) but somewhat lower than values obtained in the South Atlantic, south of the Polar Front by Rutgers van der Loeff and

BGD
8, 4871–4916, 2011

Berger, 1993. Particulate $^{231}Pa_{xs}/^{230}Th_{xs}$ (Fig. 4) is in the range of the particulate ratio observed in the Southern Ocean (Walter et al., 2001).

The averaged lithogenic contributions typically amounted for 2 % and 1 % of the dissolved and particulate $^{231}Pa_{xs}$ concentrations, respectively. The highest lithogenic contributions were observed at C1 (50 m depth, 10 % contribution) for dissolved $^{231}Pa_{xs}$ and at C11 (2000 m depth, 7 % contribution) for $^{231}Pa_{xs}$ in particles.

We are aware of the large uncertainties associated with some of the presented results (Tables 3 and 4). However, variations in the ^{230}Th and ^{231}Pa profiles can be interpreted together with other tracers, such as REEs, Si or Ra, to discuss some particular or characteristic features of the radionuclides in the Kerguelen wake.

3.1 On-plateau stations (0–560 m depth)

Dissolved $^{231}Pa_{xs}$ was analyzed at 3 of the 6 on-plateau stations (A3-33, A3-77 and C1) that were studied for $^{230}Th_{xs}$ (Table 3, Fig. 2a and for $^{230}Th_{xs}$, cf. Venchiarutti et al., 2008). At these 3 stations, dissolved $^{231}Pa_{xs}$ distribution is mainly constant all along the water column (Fig. 2a). Very low dissolved $^{231}Pa_{xs}$ concentrations are found in the surface water at station A3-33, whereas slightly higher dissolved $^{231}Pa_{xs}$ are found at A3-77 and even higher at station C1, close to Heard Island. A surprising maximum of dissolved $^{231}Pa_{xs}$ (0.079 dpm m^{-3}) is observed at 150 m depth at the plateau station A3-77 (4 February 2005; Fig. 2a).

Dissolved $^{231}Pa_{xs}/^{230}Th_{xs} \geq 0.093$ (Fig. 3a) is found in the water column at stations A3-77 and C1, whereas dissolved $^{231}Pa_{xs}/^{230}Th_{xs} \leq 0.093$ is found at A3-33 throughout most of the water column. The lowest dissolved $^{231}Pa_{xs}/^{230}Th_{xs}$ activity ratios (Fig. 3a) are found at A3-33 with an average of 0.072 ± 0.060 (2 s.d.) for the whole water column.

The average $^{231}Pa_{xs}$ concentration in particles (Table 3), measured only at station A3-77, is 0.017 dpm m^{-3} representing about 43 % of the total $^{231}Pa_{xs}$ concentration at this station. Particulate $^{231}Pa_{xs}/^{230}Th_{xs} \geq 0.093$ (Fig. 4) is observed at this latter station, with a decrease of the ratio with increasing depth.

BGD
8, 4871–4916, 2011

3.2 Off-plateau stations (0–3275 m depth)

Dissolved $^{231}Pa_{xs}$ were measured at 4 off-plateau stations (Fig. 2b): Kerfix and C11, B11 and A11 ("open ocean"-HNLC stations).

Dissolved ^{231}Pa concentrations (Table 4) increase almost linearly with depth down to 1000 m ($\sigma_0 = 27.65\,kg\,m^{-3}$), in agreement with what was already observed in the Southern Ocean (Rutgers van der Loeff and Berger, 1993; Chase et al., 2003).

However, at the off-plateau station Kerfix west of the Kerguelen plateau (Fig. 1), unlike the observed ^{230}Th linear vertical profile (cf. Venchiarutti et al., 2008), dissolved ^{231}Pa profile appears variable with depth, displaying a maximum value of $0.17\,dpm\,m^{-3}$ at 800 m depth ($\sigma = 27.62\,kg\,m^{-3}$; Table 4). A maximum was also observed at the same depth for REEs, suggesting a recent element release from sediment material deposited on the slope (Zhang et al., 2008a). Since both ^{231}Pa and REEs have longer residence times in the water column than ^{230}Th, such input would be longer captured by ^{231}Pa relative to ^{230}Th which is more rapidly scavenged.

Between 1000 m and 2500 m (Figs. 2b and 5b, $27.80 < \sigma_0 < 27.65\,kg\,m^{-3}$) at stations A11, B11 and C11 along the eastern flank of the plateau, dissolved ^{231}Pa exhibits depleted profiles deviating from the linear distribution with depth.

Close to the seafloor (Fig. 5b, $\sigma_0 \leq 27.80\,kg\,m^{-3}$), dissolved $^{231}Pa_{xs}$ concentrations are strongly depleted at stations A11, C11 and B11. However, $^{231}Pa_{xs}$ concentrations remain higher at station B11 than in any other bottom waters of the studied area (up to $0.309\,dpm\,m^{-3}$ at 2800 m depth).

Particulate $^{231}Pa_{xs}$ concentrations vary from $0.0003\,dpm\,m^{-3}$ (2000 m, C11) to $0.072\,dpm\,m^{-3}$ (80 m, C11, Table 4). Particulate $^{231}Pa_{xs}$ contributes to around 20 % of total $^{231}Pa_{xs}$, in deep waters. Most of the $^{231}Pa_{xs}$ is bound to particles in the upper 100 m of the water column only. This is the case at station C11 with a high particulate $^{231}Pa_{xs}$ contribution (~ 75 %) in the surface waters.

Dissolved and particulate $^{231}Pa_{xs}/^{230}Th_{xs}$ ratios are relatively constant with depth and ≥ 0.093 (Figs. 3b and 4, respectively), except few maxima: at station B11 for the

BGD
8, 4871–4916, 2011

dissolved phase (reaching 3.031 at the surface, Table 4) and at station C11 for particles (with a mean value of ~2.76 between 80 m and 200 m, Table 4).

4 Discussion

Here, we aimed at determining the mechanisms involved in Pa and Th scavenging, fractionation and their resulting distributions in seawater and particles in the wake of Kerguelen.

4.1 Fractionation of ^{231}Pa and ^{230}Th in the wake of Kerguelen

Dissolved $^{231}Pa_{xs}/^{230}Th_{xs}$ activity ratio does not change significantly with depth on and off the Kerguelen plateau. Contrastingly, particulate $^{231}Pa_{xs}/^{230}Th_{xs}$ activity ratio decreases by a factor of ~2 between shallow and deep waters whatever the station (Figs. 3 and 4). These variations could reflect changes in the rates of exchange processes (adsorption/desorption, aggregation/disaggregation) between particles and seawater and/or in the particles chemistry (composition or particle alteration).

Indeed, most particulate $^{231}Pa_{xs}/^{230}Th_{xs}$ ratios larger than 0.093 (Fig. 4 and Tables 3 and 4) are associated with high particulate BSi concentrations (Fig. 6, cf. also Mosseri et al., 2008). For example, the off-plateau station C11 displays the highest surface BSi concentrations of ~5 µmol L^{-1} (Mosseri et al., 2008, also represented in Fig. 6) but also the highest particulate $^{231}Pa_{xs}/^{230}Th_{xs}$ ratios (≈2.76, Table 4). Such high values in suspended particles have already been observed by Walter et al. (1997), in the upper water column during similar plankton blooms and were attributed to an increase of the opal content in the particles.

At station B11, high dissolved $^{231}Pa_{xs}/^{230}Th_{xs}$ surface values are also observed (Table 4). However, radionuclide particulate data are missing at this station, preventing us from drawing any trend between BSi and radionuclide concentrations in particles. These high surface values might result from the dissolution of opal (Fripiat et al., 2011),

BGD
8, 4871–4916, 2011

consistent with the dissolved $Si(OH)_4$ increase observed at the base of the mixed layer (Mosseri et al., 2008: up to 50 µmol L^{-1} between 80–125 m).

The fractionation factor (noted $F_{Th/Pa}$) is a good tool to investigate the influence of particle composition on the scavenging and fractionation of ^{231}Pa and ^{230}Th, assuming chemical equilibrium between dissolved and particulate phases. It provides information on the element reactivity according to the particle composition (Luo and Ku, 1999, 2004; Walter et al., 1999; Guo et al., 2002; Chase et al., 2002, 2004) and is defined as follows:

$$F_{Th/Pa} = \frac{\left(^{230}Th/^{231}Pa\right)_{part}}{\left(^{230}Th/^{231}Pa\right)_{diss}} = \frac{K_{Th}}{K_{Pa}} \quad (4)$$

Where K_{Th} and K_{Pa} are the partition coefficients for ^{230}Th and ^{231}Pa, respectively, defined as the activity ratio between particle and seawater distributions. Note that both activities are here expressed as dpm of Th and Pa per m^3 of seawater (Scholten et al., 1995; Venchiarutti et al., 2008; Roy-Barman, 2009) and not related to the mass of particles per litre of seawater (Chase et al., 2002), since no "extensive" study of the particulate composition or particle size/surface area was carried out during KEOPS cruise. Consequently, the partition coefficients determined here are dependent on the particles concentration and will change if particle mass changes.

In most of the open ocean, Th is preferentially scavenged over Pa yielding a fractionation factor $F_{Th/Pa}$ of roughly 10 (Anderson et al., 1983a). In the Kerguelen area (Fig. 7), $F_{Th/Pa}$ values are very low, ranging from 0.06 ± 0.01 (C11 200) to 2.13 ± 0.63 (1200 m, Kerfix). $F_{Th/Pa}$ close to 1 is typically observed when opal abundance is high (Walter et al., 1997; Chase et al., 2002; Scholten et al., 2005, 2008) reflecting the high affinity of Pa for opal. Moreover, the observed $F_{Th/Pa} < 1$ in the surface waters of the Kerguelen area suggests that high opal abundance favour adsorption of ^{231}Pa onto particles with more efficiency than ^{230}Th, thereby producing high particulate $^{231}Pa_{xs}/^{230}Th_{xs}$ ratios in the euphotic layer. It confirms the enhanced affinity of ^{231}Pa for opal when opal represents more than 60 % of the particulate matter (Scholten et al., 2005).

BGD
8, 4871–4916, 2011

Excellent correlation coefficients are observed between K_{Pa} and BSi, confirming that the ^{231}Pa is better absorbed when particles are opal rich (Fig. 8). Such plot was only possible for Kerfix and C11, where BSi and K_{Pa} are documented with a sufficient resolution.

Using parameter such as $F_{Pa/Th}$, K_{Th} or K_{Pa} to establish a link between the particulate matter composition and its effect on Pa and Th fractionation, we implicitly assume that Pa and Th have reached a chemical equilibrium between the dissolved and the particulate phases. However, it has been suggested that such equilibrium takes about 1000 m to be established (Thomas et al., 2006). Therefore, we must remain cautious in our interpretation.

Nevertheless, the $F_{Th/Pa}$ values and the strong correlations between K_{Pa} and BSi confirm that ^{231}Pa and ^{230}Th fractionation in the Kerguelen area appears driven by the biogenic opal content of the particles. This is consistent with the high abundance of large diatoms in the euphotic layer of the Kerguelen area (Armand et al., 2008; Carlotti et al., 2008).

4.2 Evidence of boundary scavenging along the eastern slope of the Kerguelen plateau

At the eastern off-plateau stations C11, B11 and A11, waters entrained by the Fawn Trough current (Fig. 1), flow northward along the eastern flank of the Kerguelen plateau (Park et al., 2008a; Mongin et al., 2008). In the deep waters (σ_0 = 27.65–27.84 kg m^{-3}, i.e. from 1000 m depth to the bottom) $^{231}Pa_{xs}$ concentration profiles are distinct from one another (Figs. 2b and 5a), while the deep water masses of these stations have similar θ-S characteristics (Park et al., 2008a). The $^{231}Pa_{xs}$ depletion is most pronounced at A11 and least pronounced at B11. C11 is intermediate. These features are qualitatively similar to those observed for the $^{230}Th_{xs}$ profiles at the same stations (Venchiarutti et al., 2008).

As for ^{230}Th, we attribute the $^{231}Pa_{xs}$ depletion to an intensive boundary scavenging in the water flowing along the eastern slope of the plateau, possibly due

BGD
8, 4871–4916, 2011

to particle re-suspension and/or nepheloid layers in the deep and bottom waters (Venchiarutti et al., 2008). Indeed, it has been shown (notably for ^{210}Pb) that particle re-suspension (e.g. particles supplied from the seafloor with nepheloid layers) can have a strong impact on the radionuclide scavenging in the deep ocean (Nozaki et al., 1997; Turnewitsch et al., 2008; Okubo et al., 2007), even if the exact mechanisms of this bottom scavenging (irreversible?) remain to be determined.

Although C11 seems located upstream of B11 (Fig. 1), some of the C11 deep water have already interacted with the slope sediments, which is not the case for B11 waters, located in the core of the Fawn Trough (Park et al., 2008a). A larger interaction of seawater with the sediments at station C11 compared to station B11 is also imprinted in the Nd isotopic signature of these waters (Zhang et al., 2008b). This can also explain that there is a larger depletion in the radionuclide concentration at C11 compared to B11 (Figs. 2b and 5a).

Comparing the mean dissolved $^{231}Pa_{xs}$ and $^{230}Th_{xs}$ concentrations below 1000 m at B11 and A11, we estimated that this margin effect leads to a scavenging of $\Delta^{231}Pa_{xs}$ = 82 ± 5 % and $\Delta^{230}Th_{xs}$ = 56 ± 34 % during the 370 km northward flow of the deep water masses. Similarly, the Nd concentration decreases by almost 30 % between B11 and A11 (Zhang et al., 2008b).

Assuming that these depletions are only due to scavenging on particles, the average $F_{Th/Pa}$ along the escarpment can be estimated as $(\Delta^{230}Th_{xs}/\Delta^{231}Pa_{xs})/((1 - \Delta^{230}Th_{xs})/(1 - \Delta^{231}Pa_{xs}))$ = 0.28. Taking the uncertainties on $\Delta^{230}Th_{xs}$ and $\Delta^{231}Pa_{xs}$ into account, we obtain a total range of $F_{Th/Pa}$ = 0.04–2.7. This range is consistent with the $F_{Th/Pa}$ values estimated at C11 and A11 (based on dissolved and particulate data, Fig. 7) that are all below 2, with only one value above 1, at 700 m depth at C11).

These scavenging estimates and low fractionation factor for $^{231}Pa_{xs}$ and $^{230}Th_{xs}$ confirm that in an environment dominated by BSi, ^{231}Pa removal is at least as efficient and possibly more efficient than ^{230}Th removal as we inferred in the previous section from the K_{Pa} and $F_{Th/Pa}$ data.

BGD
8, 4871–4916, 2011

Finally, in the case of the Kerguelen area, the high abundance of opal appears to enhance the "boundary scavenging" effect already generated by the difference in the radionuclide residence times (Anderson et al., 1983b).

4.3 Scavenging of ^{231}Pa on the Kerguelen plateau

We now apply the Kerguelen plateau boundary scavenging model developed for ^{230}Th (Venchiarutti et al., 2008) to ^{231}Pa, in order to determine the ^{231}Pa scavenging rate over the plateau, the influence of open ocean water advection and thereby the resulting Pa flux down to the sediment.

We assumed that between 0 and 500 m, the ^{231}Pa concentration in the open ocean essentially increases linearly with depth and took the off-plateau station B11 as reference for the open ocean with $(d^{231}\mathrm{Pa}_{\mathrm{xs-t}}/dz) = 3.3 \times 10^{-4}$ dpm m^{-2}. In order to estimate $d^{231}\mathrm{Pa}_{\mathrm{xs-t}}$ concentration at B11, particulate data missing at this station, we took the average $K_{\mathrm{Pa}} = 0.18$ at the off-plateau station Kerfix (taking all the values below 100 m depth).

The vertical dissolved Pa profile over the plateau, derived from Eq. (13) in Venchiarutti et al. (2008), is then given by:

$$^{231}\mathrm{Pa}_{\mathrm{xs-d}} = \frac{P_{^{231}\mathrm{Pa}}}{SK_{\mathrm{Pa}}A}\left(1 - e^{-Az}\right) + \frac{\tau}{SK_{\mathrm{Pa}}A^2}\left(\frac{d^{231}\mathrm{Pa}_{\mathrm{xs-t}}}{dz}\right)\left(Az - 1 + e^{-Az}\right) \quad (5)$$

Where A is a constant defined as $A = (\tau(1 + K_{\mathrm{Pa}})/SK_{\mathrm{Pa}})$, τ is the transit time of the water at station A3 defined as $\tau = L/u = 0.33$ y, taking an horizontal speed u of 5 cm s^{-1} (mean current velocity measured with moorings, for the stations of the transect A, cf. Park et al., 2008a) and a distance over the whole plateau $L = 520$ km (Venchiarutti et al., 2008). Thus, we estimated the water residence time on the plateau of about 4 months, which may be considered as the lowest value for the water residence time, since this estimate is based on the highest mean current velocity on the whole plateau.

BGD
8, 4871–4916, 2011

We assume that Th and Pa are transported on the plateau at the same particle settling velocity and hence onto the same class of settling particles ($S = 3000\,\mathrm{m\,yr^{-1}}$, Venchiarutti et al., 2008). Over the plateau, we take the mean value $K_{Pa} = 0.56 \pm 0.21$ at station A3-77. The production rate of ^{231}Pa is $P = 0.002436\,\mathrm{dpm\,m^{-3}\,yr^{-1}}$.

Despite the few available data, their general agreement with the modelled profile at station A3 confirms the importance of advection on the distribution of ^{231}Pa over the plateau (Fig. 9). The model allows us to estimate that the vertical particulate ^{231}Pa flux settling at 500 m over the plateau is $S \times (^{231}\mathrm{Pa}_{\mathrm{xs-p}})_{500\,\mathrm{m}} = 83.48\,\mathrm{dpm\,m^{-2}\,yr^{-1}}$ and represents almost 69 times the local in situ production integrated over a 500 m depth water column. This high ^{231}Pa flux is possible because the ^{231}Pa scavenging residence time ($h/(2SK_{Pa}) \sim 0.16$ y) in the water column is shorter than the residence time of the water on the Kerguelen plateau (~ 0.33 y), thereby allowing an efficient scavenging and because the advected open ocean water has a high ^{231}Pa content. Hence, the drawdown of the dissolved ^{231}Pa concentration over the plateau remains limited because advection of open ocean water brings continuously new ^{231}Pa over the plateau. If similar scavenging conditions occurred without any advection of open-ocean water, the dissolved ^{231}Pa concentration should be much lower than observed (Fig. 9, curve "plateau profile without advection", $F = 0$).

In the Panama and Guatemala Basins, the lack of Pa-Th fractionation associated with boundary scavenging of ^{230}Th and ^{231}Pa was explained by a moderately intensified scavenging compared to the open ocean with $F_{Th/Pa} \ll 10$ rather than by a quantitative stripping of ^{231}Pa and ^{230}Th with $F_{Th/Pa} = 10$ (Anderson et al., 1983b). In the Kerguelen plateau case, there is both $F_{Th/Pa} \ll 10$ (Fig. 7) and a strongly intensified scavenging due to the high biological productivity, but not completely reflected in the dissolved ^{230}Th and ^{231}Pa concentrations due to the effect of advection.

In summary, the ^{231}Pa data confirm that there is an enhanced scavenging on the plateau, as already observed for ^{230}Th (Venchiarutti et al., 2008). Moreover, ^{231}Pa concentrations showed that this intensified scavenging on the Kerguelen plateau is due to both particle flux and particle composition effects, leading to a low Pa/Th fractionation.

BGD
8, 4871–4916, 2011

However, the "boundary scavenging" model proposed for the Kerguelen plateau in Venchiarutti et al. (2008), is a particular case of boundary scavenging model where the open ocean is infinitely large compared to the ocean margin (Roy-Barman, 2009). Compared to the boundary scavenging created by a large continental margin in the Pacific Ocean as described by Bacon et al. (1988), the strong ^{230}Th and ^{231}Pa scavenging at Kerguelen (a small spot in the Southern Ocean) should not create a significant depletion of these radionuclides throughout the whole Southern Ocean.

However, these results stress that, even for particulate reactive metals with short residence time in the water column, the effect of lateral advection over the Kerguelen plateau cannot be neglected. Indeed, subsequently to the publication of the boundary scavenging model for the Kerguelen plateau, Chever et al. (2010) clearly showed that lateral advection of dissolved iron towards the Kerguelen plateau should be also considered as a predominant source of total dissolved iron (total apparent particulate iron and dissolved iron) above the plateau.

Thus, even if the "advection-scavenging model" applied to ^{230}Th and ^{231}Pa, cannot be strictly applied to other elements (like iron), it nevertheless shows that it is necessary to take this advection into account to establish the budget of other particle reactive elements, which have been treated in a one-dimensional way over the Kerguelen plateau until now (Blain et al., 2007).

5 Conclusions

In the wake of the Kerguelen plateau, $^{231}Pa_{xs}$ and $^{230}Th_{xs}$ distributions in seawater and particles and their fractionation are in the range of those previously observed in the Southern Ocean. This study showed that in the Kerguelen wake dominated by biogenic silica, ^{231}Pa removal is at least as efficient and possibly more efficient than ^{230}Th removal, thereby setting the Pa/Th ratios and fractionation factor ($F_{Th/Pa} \leq 1$) in the water column, and consequently in the sediments of this area of the Southern Ocean.

BGD
8, 4871–4916, 2011

We confirm that along the eastern plateau escarpment, an intensive scavenging occurs in the deep water as depicted by the decrease of dissolved $^{230}Th_{xs}$ and $^{231}Pa_{xs}$ concentrations between B11 and A11, a decrease which is attributed to the scavenging of more than half of the $^{230}Th_{xs}$ and $^{231}Pa_{xs}$. The lack of fractionation of $^{231}Pa_{xs}$ and $^{230}Th_{xs}$ ($F_{Th/Pa} \approx 1$) associated with this intense scavenging was attributed to nepheloid layers inducing re-suspension of BSi-rich particles stripping the deep water column of both radionuclides. To our knowledge, this work is the first conspicuous observation of boundary scavenging directly from the decrease of both dissolved ^{231}Pa and ^{230}Th concentrations when a water mass flows along an "ocean boundary".

In addition it sheds a new light on the boundary scavenging processes. Indeed, boundary scavenging, depicted in this study by changes in the fractionation of Pa and Th, occurs in the wake of Kerguelen due to the combination of both particle effect with a gradient in the particle fluxes (e.g. higher particle flux at the margin than in the open-ocean) and the effect of particle composition (dominated here by opal).

On the Kerguelen plateau, using an "advection-scavenging model", we show that the advection of open-ocean water, rich in dissolved ^{230}Th and ^{231}Pa, plays a critical role in the radionuclides budget by balancing the drawdown of both nuclides concentrations due to the intensive scavenging. Consequently, we strongly recommend that, so as to establish the distributions of other elements of interest in the water column in high scavenging areas (e.g. the Kerguelen plateau in this study), the advection of water from a lower scavenging area should be taken into account in future reversible-scavenging models.

Ultimately, the future publications on Th and Pa distributions and their fractionation in contrasted areas of the ocean will provide more realistic representations of particle composition and particle dynamics, necessary to develop a more sophisticated modelling approach of the scavenging processes of particle-reactive elements in Global Circulation Models (Dutay et al., 2009).

BGD
8, 4871–4916, 2011

Acknowledgements. We thank the captain and crew of the R/V *Marion Dufresne*, the PI of KEOPS project Stephane Blain and the chief scientist Bernard Quéguiner. We would like to thank Lionel Scouarnec and Christophe Guillerm (INSU) for their help with the in-situ pumps. We are grateful to Jean-Louis Reyss who enabled us to achieve the gamma measurements at LSM. We are especially thankful to Roger Francois and Walter Geibert for providing the Pa spikes allowing us to achieve this study. We thank Catherine Pradoux for her help in the clean laboratory. This work was supported by the IPEV (Institut Paul Emile Victor), the INSU/CNRS and the LEGOS (Toulouse).

The publication of this article is financed by CNRS-INSU.

References

Anderson, R. F., Bacon, M. P., and Brewer, P. G.: Removal of ^{230}Th and ^{231}Pa from open ocean, Earth Planet. Sci. Lett., 62, 7–23, 1983a.

Anderson, R. F., Bacon, M. P., and Brewer, P. G.: Removal of ^{230}Th and ^{231}Pa at ocean margins, Earth Planet. Sci. Lett., 66, 73–90, 1983b.

Anderson, R. F., Lao, Y., Broecker, W. S., Trumbore, S. E., Hofmann, H. J., and Wolfi, W.: Boundary scavenging in the Pacific Ocean: a comparison of ^{10}Be and ^{231}Pa, Earth Planet. Sci. Lett., 96, 287–304, 1990.

Armand, L. K., Crosta, X., Quéguiner, B., Mosseri, J., and Garcia, N.: Late summer diatom biomass and community structure on and around the naturally iron-fertilised Kerguelen Plateau in the Southern Ocean, Deep-Sea Res. Pt. II, 55, 653–676, 2008.

Bacon, M. P. and Anderson, R. F.: Distribution of thorium isotopes between dissolved and particulate forms in the deep sea, J. Geophys. Res., 87, 2045–2056, 1982.

BGD
8, 4871–4916, 2011

Bacon, M. P.: Tracers of chemical scavenging in the ocean: boundary effects and large scale chemical fractionation, Philos. Trans. R. Soc. London, A325, 147–160, 1988.
Blain, S., Quéguiner, B., Armand, L., Belviso, S., Bombled, B., Bopp, L., Bowie, A., Brunet, C., Brussaard, C., Carlotti, F., Christaki, U., Corbière, A., Durand, I., Ebersbach, F., Fuda, J.-L., Garcia, N., Gerringa, L., Griffiths, B., Guigue, C., Guillerm, C., Jacquet, S., Jeandel, C., Laan, P., Lefèvre, D., Lo Monaco, C., Malits, A., Mosseri, J., Obernosterer, I., Park, Y.-H., Picheral, M., Pondaven, P., Remenyi, T., Sandroni, V., Sarthou, G., Savoye, N., Scouarnec, L., Souhaut, M., Thuiller, D., Timmermans, K., Trull, T., Uitz, J., van Beek, P., Veldhuis, M., Vincent, D., Viollier, E., Vong, L., and Wagener, T.: Effect of natural iron fertilisation on carbon sequestration in the Southern Ocean, Nature, 446, 1070–1074, 2007.
Bradtmiller, L. I., Anderson, R. F., Fleisher, M. Q., and Burckle, L. H.: Diatom productivity in the Equatorial Pacific Ocean from the last glacial period to the present: a test of the silicic acid leakage hypothesis, Paleoceanography, 21, PA4201, doi:10.1029/2006PA001282, 2006.
Bradtmiller, L. I., Anderson, R. F., Fleisher, M. Q., and Buckle, L. H.: Comparing glacial and Holocene opal fluxes in the Pacific sector of the Southern Ocean, Paleoceanography, 24, PA2214, doi:10.1029/2008PA001693, 2009.
Carlotti, F., Thibault-Botha, D., Nowaczyk, A., and Lefevre, D.: Zooplankton community structure, biomass and role in carbon fluxes during the second half of a phytoplankton bloom in the eastern sector of the Kerguelen Shelf (January–February 2005), Deep-Sea Res. Pt. II, 55, 720–733, 2008.
Chase, Z., Anderson, R. F., Fleisher, M. Q., and Kubik, P. W.: The influence of particle composition and particle flux on scavenging of Th, Pa and Be in the ocean, Earth Planet. Sci. Lett., 204, 215–229, 2002.
Chase, Z., Anderson, R. F., Fleisher, M. Q., and Kubik, P. W.: Scavenging of ^{230}Th, ^{231}Pa and ^{10}Be in the Southern Ocean (SW Pacific sector): the importance of particle flux, particle composition and advection, Deep-Sea Res. Pt. II, 50, 739–768, 2003.
Chase, Z. and Anderson, R. F.: Comment on "On the importance of opal, carbonate, and lithogenic clays in scavenging and fractionating ^{230}Th, ^{231}Pa and ^{10}Be in the ocean" by Luo and T. L. Ku, Earth Planet. Sci. Lett., 220, 213–222, 2004.
Chever, F., Sarthou, G., Bucciarelli, E., Blain, S., and Bowie, A. R.: An iron budget during the natural iron fertilisation experiment KEOPS (Kerguelen Islands, Southern Ocean), Biogeosciences, 7, 455–468, doi:10.5194/bg-7-455-2010, 2010.
Choi, M. S., Francois, R., Sims, K., Bacon, M. P., Brown-Leger, S., Fleer, A. P., Ball, L., Schnei-

BGD
8, 4871–4916, 2011

der, D., and Pichat, S.: Rapid determination of ^{230}Th and ^{231}Pa in seawater by desolvated micro-nebulization Inductively Coupled Plasma magnetic sector mass spectrometry, Marine Chem., 76, 99–112, 2001.
Coppola, L., Roy-Barman, M., Mulsow, S., Povinec, P., and Jeandel, C.: Thorium isotopes as tracers of particles dynamics and deep water circulation in the Indian sector of the Southern Ocean (ANTARES IV), Marine Chem., 100, 299–313, 2006.
Dutay, J.-C., Lacan, F., Roy-Barman, M., and Bopp, L.: Influence of particle size and type on ^{231}Pa and ^{230}Th simulation with a global coupled biogeochemical-ocean general circulation model: a first approach, Geophys. Geochem. Geosy., 10, Q01011, doi:10.1029/2008GC002291, 2009.
Edmonds, H. N., Moran, S. B., Cheng, H., and Edwards, R. L.: ^{230}Th and ^{231}Pa in the Arctic Ocean: implications for particle fluxes and basin-scale Th/Pa fractionation, Earth Planet. Sci. Lett., 227, 155–167, 2004.
Frew, R. D., Hutchins, D. A., Nodder, S., Sanudo-Wilhelmy, S., Tovar-Sanchez, A., Leblanc, K., Hare, C. E., and Boyd, P. W.: Particulate iron dynamics during FeCycle in subantarctic waters southeast of New Zealand, Global Biogeochem. Cy., 20, GB1S93, doi:10.1029/2005GB002558, 2006.
Fripiat, F., Cavagna, A.-J., Savoye, N., Dehairs, F., André, L., and Cardinal, D.: Isotopic constraints on the Si-biogeochemical cycle of the Antarctic Zone in the Kerguelen area (KEOPS), Marine Chem., 123, 11–22, 2011.
Geibert, W. and Usbeck, R.: Adsorption of thorium and protactinium onto different particle types: experimental findings, Geochim. Cosmochim. Acta, 7, 1489–1501, 2004.
Guo, L., Chen, M., and Gueguen, C.: Control of Pa/Th ratio by particulate chemical composition in the ocean, Geophys. Res. Lett., 29(20), 1961–1963, 2002.
Hayes, C. T., Anderson, R. F., and Fleisher, M. Q.: Opal accumulation rates in the equatorial Pacific and mechanisms of deglaciation, Paleoceanography, 26, PA1207, doi:10.1029/2010PA002008, 2011.
Jacquet, S. H. M., Cardinal, D., Savoye, N., Obernosterer, I., Christaki, U., Monnin, C., and Dehairs, F.: Mesopelagic organic carbon remineralization in the Kerguelen Plateau region tracked by biogenic particulate Ba, Deep-Sea Res. Pt. II, 55, 868–879, 2008.
Jeandel, C., Venchiarutti, C., Bourquin, M., Pradoux, C., Lacan, F., van Beek, P., and Riotte, J.: Single column sequential extraction of Ra, Nd, Th, Pa and U from a natural sample, Geostand. Geoanal. Res., doi:0.1111/j.1751-908X.2010.00087.x, 2011.

BGD
8, 4871–4916, 2011

Luo, S., Ku, T.-L., and Kusabe, M.: Tracing particle cycling in the upper ocean with ^{230}Th and ^{228}Th: an investigation in the Equatorial Pacific along 140° W, Deep-Sea Res. Pt. II, 42, 805–829, 1995.
Marchal, O., François, R., and Scholten, J.: Contribution of ^{230}Th measurements to the estimation of the abyssal circulation, Deep-Sea Res. Pt. I, 54, 557–885, 2007.
Marinov, I., Gnanadesikan, A., Toggweiler, J. R., and Sarmiento, J. L.: The Southern Ocean biogeochemical divide, Nature, 441, 964–967, 2006.
Mongin, M., Molina, E., and Trull, T. W.: Seasonality and scale of the Kerguelen Plateau phytoplankton bloom: a remote sensing and modeling analysis of the influence of natural iron fertilization in the Southern Ocean. Deep-Sea Res. Pt. II, 55, 880–892, 2008.
Moran, S. B., Charette, M. A., and Hoff, J. A.: Distribution of ^{230}Th in the Labrador Sea and its relation to ventilation, Earth Planet. Sci. Lett., 150, 151–160, 1997.
Moran, S. B., Shen, C.-C., Edmonds, H. N., Weinstein, S. E., Smith, J. N., and Edwards, R. L.: Dissolved and particulate ^{231}Pa and ^{230}Th in the Atlantic Ocean: constraints on intermediate/deep water age, boundary scavenging and ^{231}Pa/^{230}Th fractionation, Earth Planet. Sci. Lett., 203, 999–1014, 2002.
Moran, S. B., Shen, C.-C., Edwards, R. L., Edmonds, H. N., Scholetn, J. C., Smith J. N., and Ku, T.-L.: ^{231}Pa and ^{230}Th in surface sediments of Arctic Ocean: implications for ^{231}Pa/^{230}Th fractionation, boundary scavenging, and advective export, Earth Planet. Sci. Lett., 234, 235–248, 2005.
Mosseri, J., Quéguiner, B., Armand, L., and Cornet-Barthaux, V.: Impact of iron on silicon utilization by diatoms in the Southern Ocean: a case study of the Si/N cycle decoupling in a naturally iron-enriched area, Deep-Sea Res. Pt. II, 55, 801–819, 2008.
Nozaki, Y. and Horibe, Y.: The water column distributions of thorium isotopes in the Western North Pacific, Earth Planet. Sci. Lett., 54, 203–216, 1981.
Nozaki, Y. and Nakanishi, T.: ^{231}Pa and ^{230}Th profiles in the open ocean water column, Deep-Sea Res., 32, 1209–1220, 1985.
Nozaki, Y., Zhang, J., and Takeda, A.: ^{210}Pb and ^{210}Po in the Equatorial Pacific and the Bering Sea: the effects of biological productivity and boundary scavenging, Deep-Sea Res. Pt. II, 44, 2203–2220, 1997.
Obernosterer, I., Christaki, U., Lefèvre, D., Catala, P., Van Wambeke, F., and Lebaron, P.: Rapid bacterial mineralization of organic carbon produced during a phytoplankton bloom induced by natural iron fertilization in the Southern Ocean, Deep-Sea Res. Pt. II, 55, 777–789, 2008.

BGD
8, 4871–4916, 2011

Okubo, A., Obata, H., Gamo, T., Minami, H., and Yamada, M.: Scavenging of ^{230}Th in the Sulu Sea, Deep-Sea Res. Pt. II, 54, 50–59, 2007.

Park, Y.-H., Roquet, F., Fuda, J. L., and Durand, I.: Circulation over and around the Kerguelen Plateau, Deep-Sea Res. Pt. II, 55, 566–581, 2008a.

Pichat, S.: Variations du rapport $(^{231}Pa/^{230}Th)_{xs,0}$ et de la composition isotopique du zinc dans des sédiments de l'océan Pacifique équatorial au Quaternaire. Implications pour la productivité biologique et relations avec la thermocline. Ph.D. thesis, Ecole Normale Supérieure de Lyon, Laboratoire des Sciences de la Terre, 2001.

Pichat, S., Sims, K. W. W., François, R., McManus, J. F., Brown-Leger, S., and Albarède, F.: Lower export production during glacial periods in the equatorial Pacific derived from $(^{231}Pa/^{230}Th)_{xs,0}$ measurements in deep-sea sediments, Paleoceanography, 19, PA4023, doi:10.1029/2003PA000994, 2004.

Pollard, R. T., Salter, I., Sanders, R. J., Lucas, M. I., Moore, M. C., Mills, R. A., Statham, P. J., Allen, J. T., Baker, A. R., Bakker, D. C. E., Charette, M. A., Fielding, S., Fones, G. R., French, M., Hickman, A. E., Holland, R. J., Hughes, J. A., Jickells, T. D., Lampitt, R. S., Morris, P. J., Nédélec, F. H., Nielsdóttir, M., Planquette, H., Popova, E. E., Poulton, A. J., Read, J. F., Seeyave, S., Smith, T., Stinchcombe, M., Taylor, S., Thomalla, S., Venables, H. J., Williamson, R., and Zubkov, M. V.: Southern Ocean deep-water carbon export enhanced by natural iron fertilization. Nature, 457, 577–580, 2009.

Regelous, M., Turner, S. P., Elliott, T. R., Rostami, K., and Hawkesworth, C. J.: Measurements of femtogram quantities of protactinium in silicate rock samples by multicollector inductively coupled plasma mass spectrometry, Anal. Chem., 54, 1142–1147, 2004.

Roy-Barman, M., Chen, J. H., and Wasserburg, G. J.: ^{230}Th-^{232}Th systematics in the Central Pacific Ocean: the sources and the fates of thorium, Earth Planet. Sci. Lett., 139, 351–363, 1996.

Roy-Barman, M., Coppola, L., and Souhaut, M.: Thorium isotopes in the Western Mediterranean Sea: insight into the marine particle dynamics, Earth Planet. Sci. Lett., 196, 161–174, 2002.

Roy-Barman, M., Jeandel, C., Souhaut, M., Rutgers van der Loeff, M. M., Voege, I., Leblond, N., and Freydier, R.: The influence of particle composition on thorium scavenging in the NE Atlantic ocean (POMME experiment), Earth Planet. Sci. Lett., 240, 681–693, 2005.

Roy-Barman, M.: Modelling the effect of boundary scavenging on Thorium and Protactinium profiles in the ocean, Biogeosciences, 6, 3091–3107, doi:10.5194/bg-6-3091-2009, 2009.

BGD
8, 4871–4916, 2011

Rutgers van der Loeff, M. M. and Berger, G. W.: Scavenging of ^{230}Th and ^{231}Pa near the Antarctic Polar Front in the South Atlantic, Deep-Sea Res. Pt. I, 40, 339–357, 1993.

Rutgers van der Loeff, M. M. and Moore, W. S.: Determination of natural radioactive tracers. Methods of Seawater Analysis, Chapter 13, 3 Edn., Verlag Chemie, Weinheim, 365– 397, 1999.

Sarmiento, J. L., Hughes, T. M. C., Stouffer, R. J., and Manabe, S.: Simulated response of the ocean carbon cycle to anthropogenic climate warming, Nature, 393, 245–249, 1998.

Savoye, N., Trull, T. W., Jacquet, S. H. M., Navez, J., and Dehairs, F.: ^{234}Th-based export fluxes during a natural iron fertilization experiment in the Southern Ocean (KEOPS), Deep-Sea Res. Pt. II, 55, 841–855, 2008.

Scholten, J. C., Rutgers van der Loeff, M. M., and Michel, A.: Distribution of ^{230}Th and ^{231}Pa in the water column in relation to the ventilation of the deep Arctic basins, Deep-Sea Res. Pt. II, 42, 1519–1531, 1995.

Scholten, J. C., Fietzke, J., Mangini, A., Stoffers, P., Rixen, T., Gaye-Haake, B., Blanz, T., Ramaswamy, V., Sirocko, F., Schulz, H., and Ittekkot, V.: Radionuclide fluxes in the Arabian Sea: the role of particle composition, Earth Planet. Sci. Lett., 230, 319–337, 2005.

Scholten, J. C., Fietzke, J., Mangini, A., Garbe-Schönberg, C.-D., Eisenhauer A., Schneider, R., and Stoffers, P.: Advection and scavenging: effects on ^{230}Th and ^{231}Pa distribution off Southwest Africa, Earth Planet. Sci. Lett., 271, 159–169, 2008.

Spencer, D. W., Bacon, M. P., and Brewer, P. G.: Models of the distribution of ^{210}Pb in a section across the North Equatorial Atlantic Ocean, J. Marine Res., 39, 119–138, 1981.

Tachikawa, K.: Apport de concentrations de Terres Rares et des compositions isotopiques de Néodyme à l'étude de processus dans la colonne d'eau: cas de l'Atlantique Tropical Nord-Est (sites EUMELI). Ph.D. thesis, Université Toulouse III, France, 1997.

Thomas, A. L., Henderson, G. M., and Robinson, L. F.: Interpretation of the ^{231}Pa/^{230}Th paleocirculation proxy: new water-column measurements from the Southwest Indian Ocean, Earth Planet. Sci. Lett., 241, 493–504, 2006.

Tréguer, P. and Pondaven, P.: Climatic changes and the carbon cycle in the SouthernOcean: a step forward, Deep-Sea Res. Pt. II, 49, 1597–1600, 2002.

Turnewitsch, R., Reyss, J.-L., Nycander, J., Waniek, J. J., and Lampitt, R. S.: Internal tides and sediment dynamics in the deep sea – evidence from radioactive ^{234}Th/^{238}U disequilibria, Deep-Sea Res. Pt. I, 55, 1727–1747, 2008.

BGD

8, 4871–4916, 2011

van Beek, P., Bourquin, M., Reyss, J.-L., Souhaut, M., Charrette, M. A., and Jeandel, C.: Radium isotopes to investigate the water mass pathways on the Kerguelen Plateau (Southern Ocean), Deep-Sea Res. Pt. II, 55, 622–637, 2008.

Venchiarutti, C., Jeandel, C., and Roy-Barman, M.: Particle dynamics study in the wake of Kerguelen Island using thorium isotopes, Deep-Sea Res. Pt. I, 55, 1343–1363, 2008.

Vogler, S., Scholten, J., Rutgers van der Loeff, M. M., and Mangini, A.: ^{230}Th in the Eastern North Atlantic: the importance of water mass ventilation in the balance of ^{230}Th, Earth Planet. Sci. Lett., 156, 61–74, 1998.

Walter, H. J., Rutgers van der Loeff, M. M., and Hoeltzen, H.: Enhanced scavenging of ^{231}Pa relative to ^{230}Th in the South Atlantic south of the Polar Front: implications for the use of the ^{231}Pa/^{230}Th ratio as a paleoproductivity proxy, Earth Planet. Sci. Lett., 149, 85–100, 1997.

Walter, H. J., Rutgers van der Loeff, M. M., and Francois, R.: Reliability of the ^{231}Pa/^{230}Th activity ratio as a tracer for bioproductivity of the ocean, in: Use of Proxies in Paleoceanography: Examples from the South Atlantic, edited by: Fischer, G. and Wefer, G., Springer-Verlag, Berlin, 393–408, 1999.

Walter, H. J., Geibert, W., Rutgers van der Loeff, M. M., Fischer, G., and Bathmann, U.: Shallow vs. deep-water scavenging of ^{231}Pa and ^{230}Th in radionuclide enriched waters of Atlantic sector of Southern Ocean. Deep-Sea Res. Pt. I, 48, 471–493, 2001.

Yu, E.-F., Francois, R., Bacon, M. P., Honjo, S., Fleer, A. P., Manganini, S. J., Rutgers van der Loeff, M. M., and Ittekot, V.: Trapping efficiency of bottom-tethered sediment traps estimated from intercepted fluxes of ^{230}Th and ^{231}Pa, Deep-Sea Res. Pt. I, 48, 865–889, 2001.

Zhang, Y., Lacan, F., and Jeandel, C.: Dissolved Rare Earth Elements trace lithogenic inputs over the Kerguelen plateau (Southern Ocean), Deep-Sea Res. Pt. II, 55(5-7), 638–652, 2008a.

Zhang, Y., Jeandel, C., and Lacan, F.: Boundary exchange processes on and along the Kerguelen plateau, Geochim. Cosmochim. Ac., 72, A12, 2008b.

BGD
8, 4871–4916, 2011

Table 1. Overall recovery range (sum of co-precipitation and chromatographic separation) obtained by Isotope Dilution (Right column). Average recovery values are reported into brackets. Pa co-precipitation recoveries were estimated with gamma-spectrometry based on 9 samples at station A3-33.

Sample types	Co-precipitation recoveries	Overall recoveries
Dissolved ^{230}Th, ^{232}Th	Not determined	10–93 % (43 ± 19 %)
Particulate ^{230}Th, ^{232}Th	X	54–103 % (90 ± 8 %)
Dissolved ^{231}Pa	103 ± 11 %	14–97 % (53 ± 4 %)[a]
Particulate ^{231}Pa	X	5–51 % (24 ± 5 %)

[a] These recoveries do not take into account the samples from stations A3-33, Kerfix and A11, since there are no overall recovery at these stations.

BGD
8, 4871–4916, 2011

Table 2. Summary of the different chemical blank contributions to seawater and particles samples, for different types of filters and for the yield tracers ^{229}Th and ^{233}Pa used for KEOPS samples. *N* is the number of samples analysed. For more details, please refer to the text Sect. 2.4.3.

Blank types	^{230}Th (fg)		^{231}Pa (fg)		*N*
	Mean	Error	Mean	Error	
Filter blanks (Versapore ⌀ 293 mm) + reactants (contribution to particles)	5.7	2.3	0.30	0.19	2
Filter blanks (Durapore) + reactants (contribution to dissolved)	1.21	0.29	1.75	0.29	1
Filter blanks (Versapore 2) + reactants (contribution to dissolved)	1.24	0.8	0.55	0.27	1
^{229}Th Spike blank	0.8	0.4	No contribution		4
^{233}Pa Spike blank (second spike)	0.32	0.11	1.28	0.15	4
	insignificant contribution				

BGD
8, 4871–4916, 2011

Table 3. Kerguelen plateau stations: dissolved and particulate $^{231}Pa_{xs}$ concentrations in dpm m^{-3} and corresponding $^{231}Pa_{xs}/^{230}Th_{xs}$ activity ratios. Oiso (as Niskin number) stands here for the ship seawater intake (OISO program). For ^{230}Th and ^{231}Pa lithogenic contributions, please refer to Venchiarutti et al. (2008) and Sect. 3 of the present text, respectively. Errors (2σ) are further described in Sect. 2.4.3. All the activities that fall outside the sensible values (e.g. negative values) are discarded.

Depth (m)		diss $^{231}Pa_{xs}$ (dpm m^{-3}) Concentration	Error	diss ($^{231}Pa/^{230}Th)_{xs}$ Activity ratio	Error	Depth (m)		Part $^{231}Pa_{xs}$ (dpm m^{-3}) Concentration	Error	Part ($^{231}Pa/^{230}Th)_{xs}$ Activity ratio	Error
Station A3-33 (Bottom: 520 m) (24 Jan 2005, 72.006° E, 50.711° S)											
20	21_23	0.001	0.008	0.004	0.032						
50	18_20	–	–	–	–						
100	15_17	0.001	0.007	0.007	0.063						
130	13_14	0.009	0.011	0.126	0.174						
200	10_12	0.004	0.007	0.009	0.018						
300	7_9	0.033	0.019	0.213	0.125						
400	4_6	0.018	0.013	0.077	0.056						
480	1_3	0.009	0.011	0.033	0.043						
Station A3-77 (Bottom: 525 m) (4 Feb 2005, 72.084° E, 50.657° S)						Station A3-77 (4 Feb 2005, 72.084° E, 50.657° S)					
0	oiso	0.030	0.055	0.733	1.343						
20	22_24	0.026	0.016	0.628	0.410						
50	19_21	0.020	0.021	0.456	0.483	pis 004	50	–	–	–	–
100	16_18	0.019	0.018	0.441	0.447						
150	13_15	0.079	0.007	0.715	0.125	pis 004	150	0.0249	0.0010	0.679	0.044
250	10_12	0.023	0.006	0.181	0.055	pis 004	250	0.0164	0.0008	0.512	0.050
350	7_9	0.016	0.006	0.083	0.033	pis 004	350	0.0102	0.0006	0.258	0.021
400	4_6	–	–	–	–						
450	1_3	0.044	0.006	0.286	0.062						
Station C1 (Bottom: 150 m) (8 Feb 2005, 73.883° E, 53.186° S)											
0	oiso	0.030	0.030	1.341	1.357						
30	18_20	0.029	0.007	0.596	0.145						
50	13_15	0.017	0.007	0.353	0.160						
100	6_8	0.028	0.008	0.460	0.143						
130	1_3	0.041	0.006	0.725	0.140						

BGD
8, 4871–4916, 2011

Table 4. Kerguelen off plateau stations: dissolved and particulate $^{231}Pa_{xs}$ concentrations in dpm m^{-3} and corresponding $^{231}Pa_{xs}/^{230}Th_{xs}$ activity ratios. For ^{230}Th and ^{231}Pa lithogenic contributions, please refer to Venchiarutti et al. (2008) and Sect. 3 of the present text, respectively. Errors (2σ) are further described in Sect. 2.4.3. In the 1st column, "pis" refers to the number of the in-situ pump deployment. All the activities that fall outside the sensible values (e.g. negative values) are discarded.

Depth (m)		diss $^{231}Pa_{xs}$ (dpm m^{-3}) Concentration	Error	diss $(^{231}Pa/^{230}Th)_{xs}$ Activity ratio	Error	Depth (m)		Part $^{231}Pa_{xs}$ (dpm m^{-3}) Concentration	Error	Part $(^{231}Pa/^{230}Th)_{xs}$ Activity ratio	Error
Station A11 (Bottom: 2600 m) (21 Jan 2005, 74.007° E, 49.013° S)						Station A11 (21 Jan 2005, 74.007° E, 49.013° S)					
60	*x*	0.007	0.010	0.023	0.032						
100	5_7	0.013	0.010	0.133	0.101						
200	22_24	0.033	0.026	0.064	0.050	pis 001	200	0.0084	0.0005	0.326	0.040
500	*x*	–	–	–	–	pis 001	300	0.0084	0.0003	0.480	0.043
800	7_9	0.079	0.025	0.164	0.053	pis 001	700	0.0119	0.0005	0.249	0.015
1500	4_6	0.034	0.013	0.115	0.043	pis 001	1500	0.0105	0.0004	0.143	0.006
2500	1_3	0.014	0.009	0.092	0.061						
Station B11 (Bottom: 3275 m) (29 Jan 2005, 76.98° E, 50.52° S)											
0	oiso	0.218	0.026	3.031	0.562						
50	22_24	0.065	0.008	0.709	0.112						
150	19_21	0.050	0.007	0.298	0.047						
300	16_18	0.085	0.006	0.284	0.026						
700	13_15	0.187	0.011	0.390	0.028						
1000	10_12	0.211	0.008	0.296	0.018						
2000	7_9	0.303	0.012	0.390	0.023						
2800	4_6	0.309	0.012	0.362	0.021						
3146	1_3	0.205	0.010	0.210	0.013						
Station C11 (Bottom: 3250 m) (28 Jan 2005, 77.965° E, 51.66° S)						Station C11 (28 Jan 2005, 77.965° E, 51.66° S)					
50	22_24	0.023	0.016	0.224	0.159	pis 002	80	0.0716	0.0027	2.648	0.136
300	16_18	0.054	0.008	0.184	0.029	pis 002	200	0.0643	0.0028	2.867	0.317
700	13_15	0.102	0.005	0.205	0.015	pis 002	700	0.0050	0.0002	0.131	0.008
1000	10_12	0.144	0.029	0.272	0.056						
2000	7_9	0.142	0.029	0.178	0.037	pis 002	2000	0.00034	0.00002	0.0042	0.0003
2800	4_6	0.230	0.010	0.314	0.017						
3180	1_3	0.154	0.008	0.244	0.017	pis 002	3200	–	–	–	–

BGD
8, 4871–4916, 2011

Table 4. Continued.

Depth (m)		diss $^{231}Pa_{xs}$ (dpm m^{-3}) Concentration	Error	diss ($^{231}Pa/^{230}Th)_{xs}$ Activity ratio	Error	Depth (m)		Part $^{231}Pa_{xs}$ (dpm m^{-3}) Concentration	Error	Part ($^{231}Pa/^{230}Th)_{xs}$ Activity ratio	Error
Station Kerfix (Bottom: 1676 m) (10 Feb 2005, 68.435° E, 50.68° S)						Station Kerfix (10 Feb 2005, 68.435° E, 50.68° S)					
0	oiso	0.029	0.014	0.676	0.339						
100	18_20	0.001	0.019	0.031	0.528	pis 006	100	0.0051	0.0006	0.503	0.326
200	15_17	0.012	0.013	0.113	0.118	pis 006	200	0.0064	0.0003	0.578	0.055
500	12_14	0.056	0.023	0.256	0.103	pis 006	500	0.0041	0.0002	0.158	0.010
800	9_11	0.172	0.010	0.576	0.047	pis 006	800	0.0103	0.0006	0.309	0.022
1200	6_8	0.154	0.045	0.347	0.100	pis 006	1200	0.0080	0.0005	0.163	0.010
1550	1_5	0.188	0.044	0.361	0.084						

BGD
8, 4871–4916, 2011

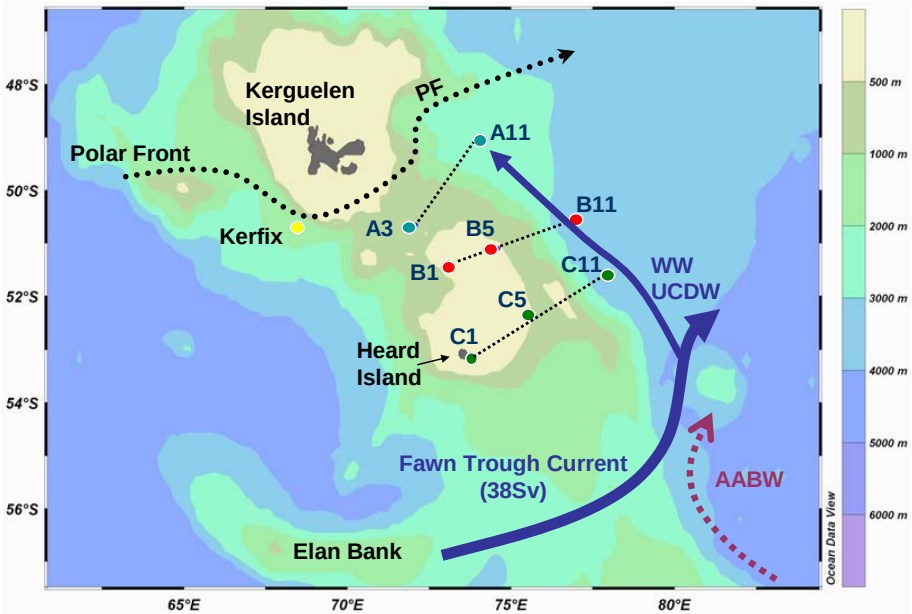

Fig. 1. Sample location and major hydrographical features during KEOPS (inspired from Park et al., 2008a). Blue arrow: Winter Water and Upper Circumpolar Deep Water flowing through the Fawn Trough and spreading north towards station A11. Dotted purple arrow: Antarctic Bottom Waters coming from the Adélie Coast. This figure was realised using Ocean Data View (Schlitzer, R., http://odv.awi.de, 2011).

BGD
8, 4871–4916, 2011

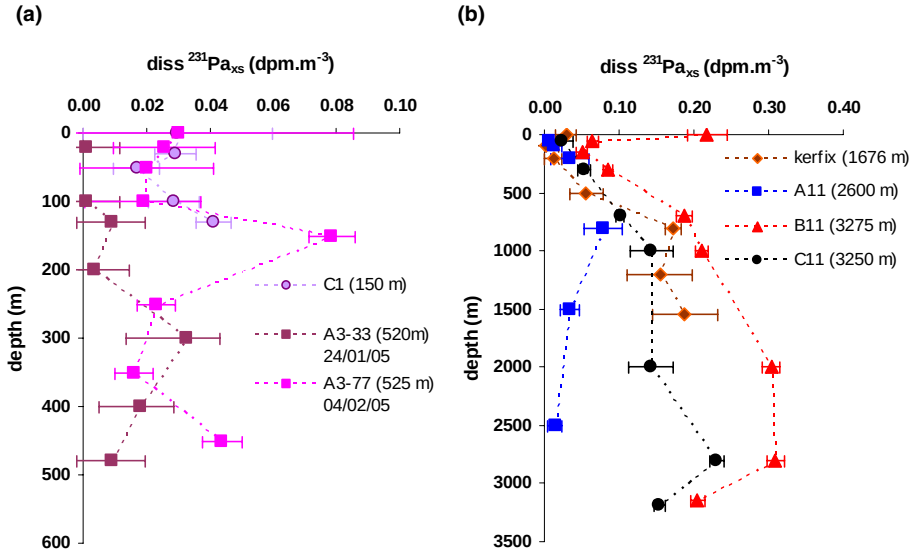

Fig. 2. Dissolved $^{231}Pa_{xs}$ vertical profiles in dpm m^{-3}. **(a)** At the Kerguelen plateau stations. **(b)** At the off-plateau stations. The error bars are represented here at the 2σ uncertainty (as described in Sect. 2.4.3). Note that for A3-33 and A3-77, sampling dates are indicated and that bottom depths at all the stations are into brackets. The concentrations may be converted from dpm m^{-3} assuming a correction of the density of seawater (i.e. $\rho = 1.027$ kg m^{-3}), we have for both $^{230}Th_{xs}$ (1 fg kg^{-1} = 0.047 dpm m^{-3}) and $^{231}Pa_{xs}$ (1 fg kg^{-1} = 0.1078 dpm m^{-3}), and for ^{232}Th (1 pg kg^{-1} = 0.00025 dpm m^{-3}).

BGD
8, 4871–4916, 2011

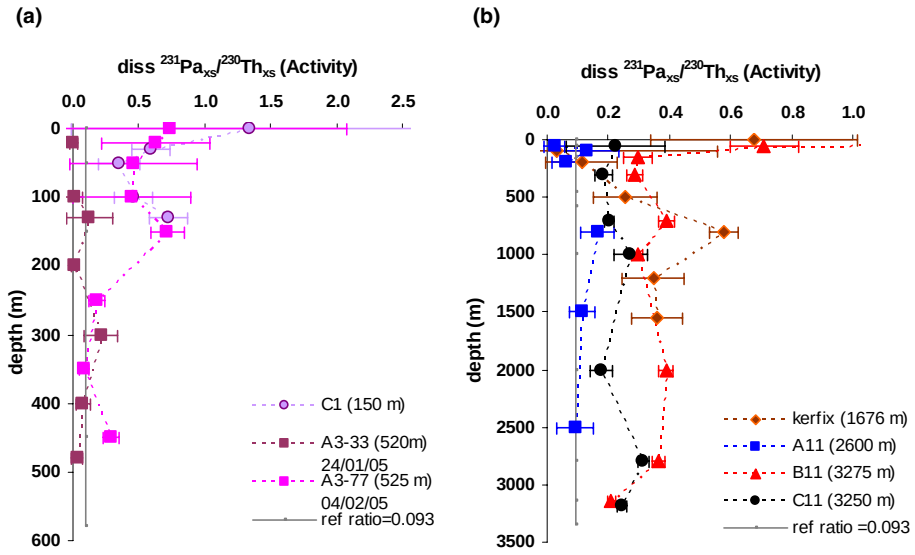

Fig. 3. Dissolved $^{231}Pa_{xs}/^{230}Th_{xs}$ activity ratio vertical profiles. **(a)** On the Kerguelen plateau. **(b)** Off-plateau. The error bars are represented here at the 2σ uncertainty (as described in Sect. 2.4.3). The grey line represents the $^{231}Pa/^{230}Th$ production activity ratio = 0.093. Bottom depths are indicated into brackets. Note that for station B11 the high dissolved ratio (3.0 ± 0.6) at the surface is not represented in this figure.

BGD
8, 4871–4916, 2011

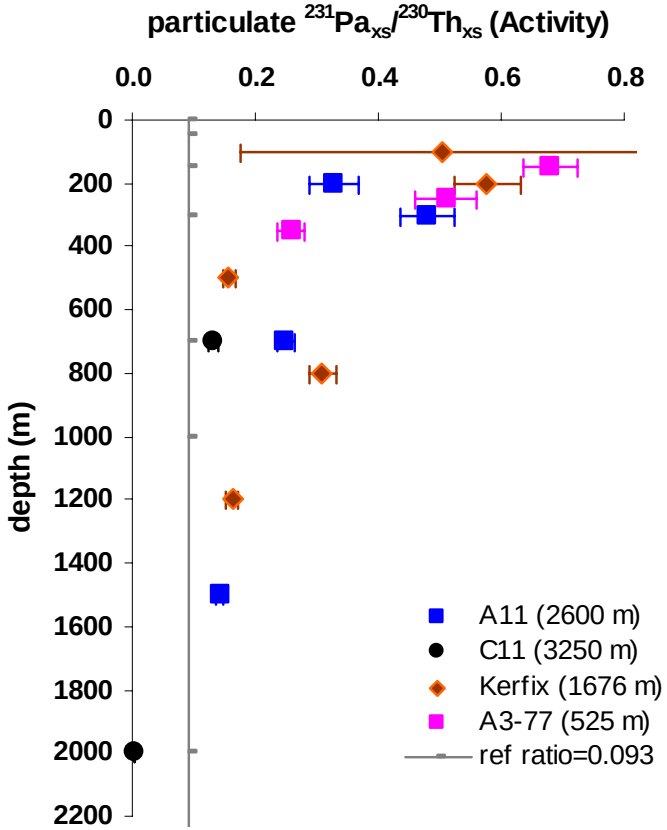

Fig. 4. Distribution of particulate $^{231}Pa_{xs}/^{230}Th_{xs}$ activity ratios (2σ error bars) with depth, on and off the Kerguelen plateau. For grey line and bottom depths, see caption of Fig. 3. Note that for station C11 the high particulate ratios (2.6 and 2.9) at the surface are not represented in this figure.

BGD
8, 4871–4916, 2011

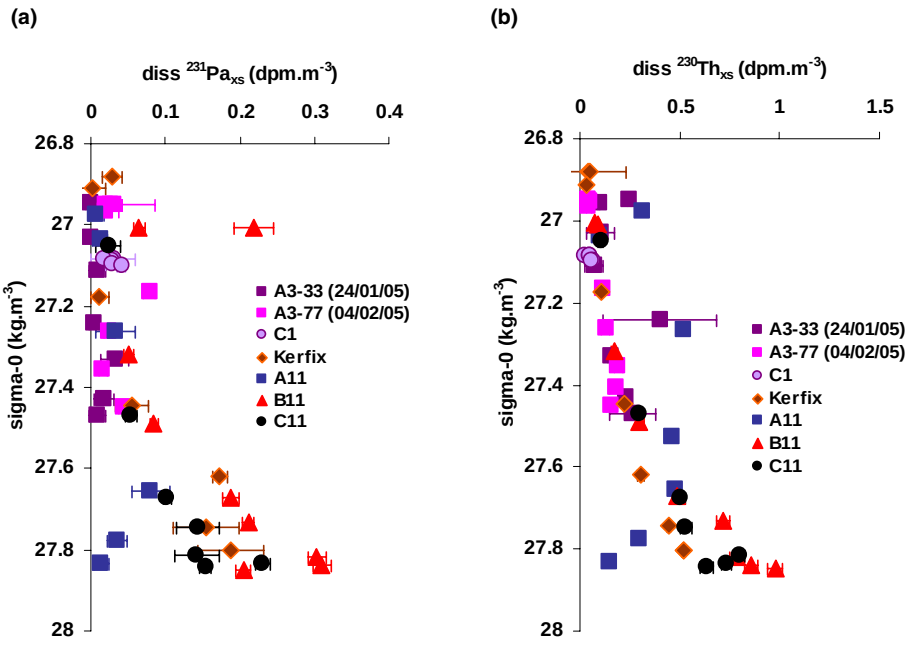

Fig. 5. Distributions with sigma-0 density (kg m^{-3}) of **(a)** dissolved $^{230}Th_{xs}$ and **(b)** dissolved $^{231}Pa_{xs}$ concentrations in dpm m^{-3}, on and off the Kerguelen plateau, during KEOPS cruise.

BGD
8, 4871–4916, 2011

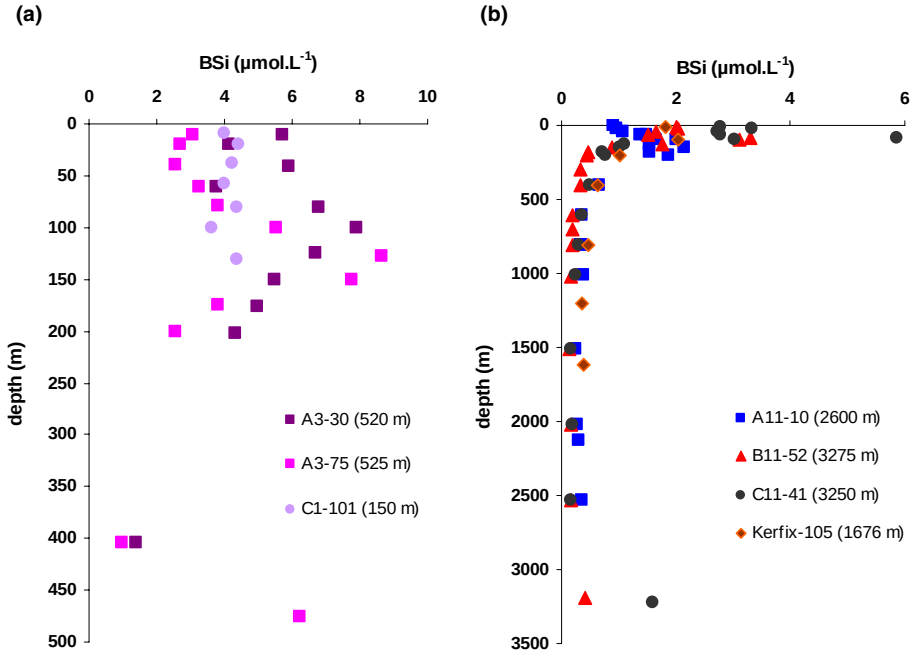

Fig. 6. Vertical profiles of the BSi (in µmol L^{-1}) acquired by and reported in Mosseri et al. 2008 during the KEOPS cruise. **(a)** Plateau stations and **(b)** off-plateau stations. The CTD number for BSi sampling is indicated next to the station name and bottom depths are given into brackets.

BGD
8, 4871–4916, 2011

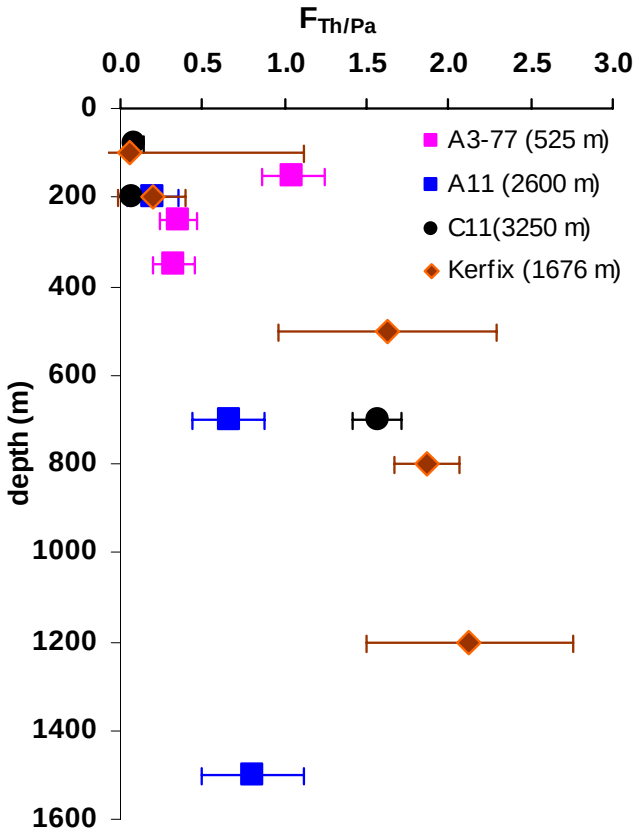

Fig. 7. Fractionation factor $F_{Th/Pa}$ distribution in the upper 1600 m depth, on and off the Kerguelen plateau, south of the Polar Front. The $F_{Th/Pa}$ factor is in the range of those observed in presence of opal material (Walter et al., 1997; Chase et al., 2002; Geibert and Usbeck, 2004). Bottom depths are indicated into brackets.

BGD
8, 4871–4916, 2011

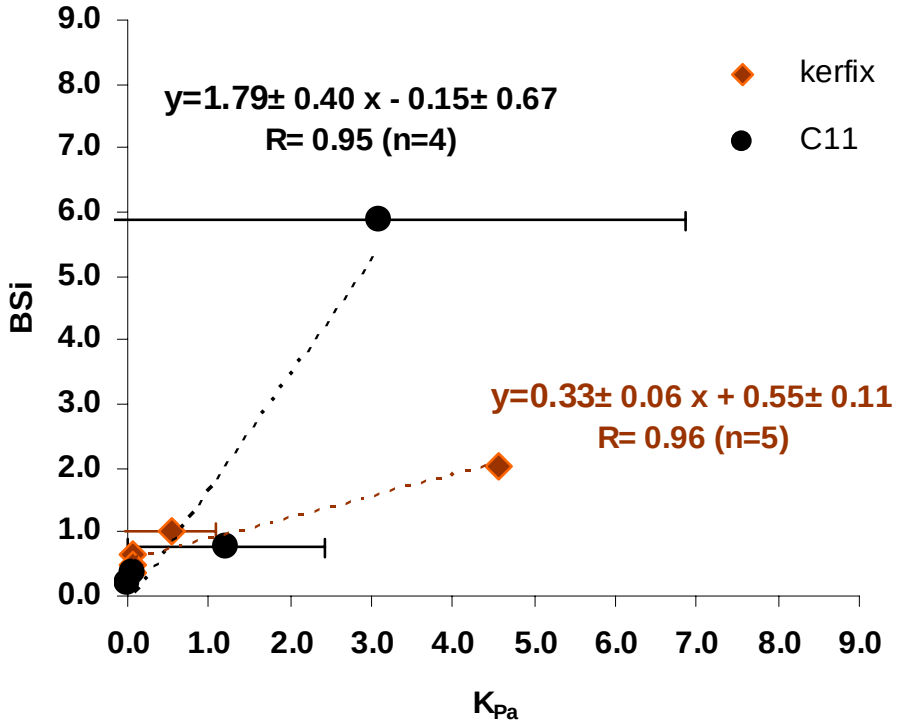

Fig. 8. Protactinium partition coefficients K_{Pa} (defined as the ratio of the particulate to dissolved ^{231}Pa activity in dpm m^{-3} of seawater) with biogenic opal content (BSi in µmol L^{-1}, from Mosseri et al., 2008) at two "open ocean" stations: Kerfix (represented here between 0–1200 m, R = 0.96) and C11 (between 0–2000 m, R = 0.95). Note that for Kerfix station, the error bar at 100 m for K_{Pa} was arbitrarily omitted in the graph since it is too large to be properly plotted.

BGD
8, 4871–4916, 2011

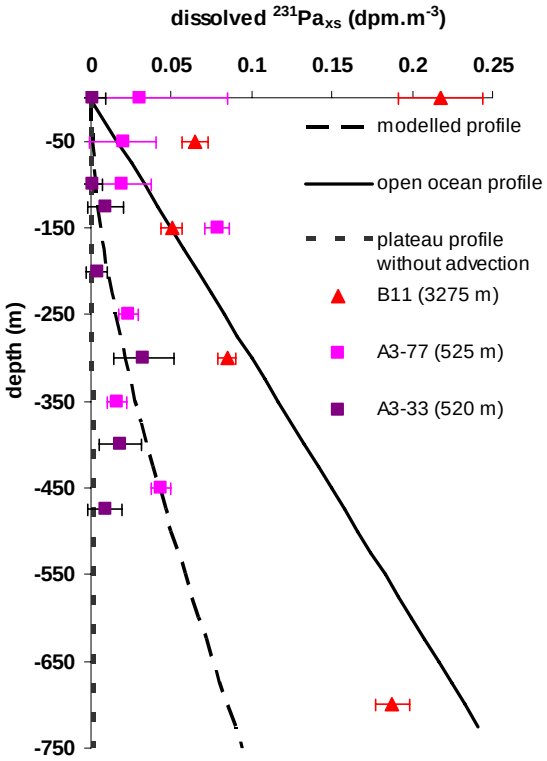

Fig. 9. Advection-scavenging model applied to dissolved $^{231}Pa_{xs}$. The symbols represent the measured dissolved $^{231}Pa_{xs}$ profiles at KEOPS stations. The lines represent: dashed line (scavenging model with advection on the plateau – A3 stations – of open-ocean water with $^{231}Pa_{xs}$ concentration increasing with depth), solid bold line (the imposed open-ocean dissolved $^{231}Pa_{xs}$ profile: B11 chosen here as reference) and dotted line (dissolved $^{231}Pa_{xs}$ profile without advection). Error bars are represented at the 2σ value. Bottom depths are indicated into brackets.

BGD
8, 4871–4916, 2011